Halloysite Tubes as Nanocontainers for Anticorrosion Coating with Benzotriazole

Elshad Abdullayev,[†] Ronald Price,[‡] Dmitry Shchukin,[§] and Yuri Lvov*[,†]

Institute for Micromanufacturing, Louisiana Technical University, Ruston, Louisiana, Glen Muir Technologies Incorporated, 114 Monopanson Drive, Stevensville, Maryland, and Max Planck Institute for Colloids and Interfaces, Golm/Potsdam, Germany

ABSTRACT Halloysite clay nanotubes were investigated as a tubular container for the corrosion inhibitor benzotriazole. Halloysite is a naturally occurring cylindrical clay mineral with an internal diameter in the nanometer range and a length up to several micrometers, yielding a high-aspect-ratio hollow tube structure. Halloysite may be used as an additive in paints to produce a functional composite coating material. A maximum benzotriazole loading of 5% by weight was achieved for clay tubes of 50 nm external diameters and lumen of 15 nm. Variable release rates of the corrosion inhibitor were possible in a range between 5 and 100 h, as was demonstrated by formation of stoppers at tube openings. The anticorrosive performance of the sol−gel coating and paint loaded with 2−5% of halloysite-entrapped benzotriazole was tested on copper and on 2024-aluminum alloy by direct exposure of the metal plates to corrosive media. Kinetics of the corrosion spot formation at the coating defects was analyzed by the scanning vibrating electrode technique, and an essential damping of corrosion development was demonstrated for halloysite-loaded samples.

KEYWORDS: halloysite • benzotriazole • corrosion protection • clay nanotubes • coatings

INTRODUCTION

Corrosion of metals is a serious technological problem, and a variety of methods such as cathodic protection, insulating coatings, and corrosion inhibition were developed to overcome it. An inhibitor-enhanced coating is one of the most efficient methods. Different types of inorganic corrosion inhibitors include chromates, phosphates, molybdates, and nitrites (1). One of the main disadvantages of inorganic inhibitors is their toxicity; for example, chromates are proven to cause several diseases, including cancer, and are recently forbidden for common usage (2). Therefore, an introduction of environmentally friendly corrosion inhibitors for protective coatings is important. Benzotriazole and its derivatives are among the most effective inhibitors used for protection of metals, especially copper and transition metals (2−17). Although benzotriazole is an efficient corrosion inhibitor for these metals, in real environments, such as chloride-containing aggressive media (e.g., seawater), its corrosion-inhibitive performance is not sufficient and combination of corrosion inhibition with passive protection (such as paint coating) is required. A direct addition of benzotriazole into the paint is not effective, because it is water-soluble and leaves empty voids in the coating layer, which decreases the barrier properties of the coating.

An introduction of benzotriazole into paint within nano- or microscale encapsulating systems drastically improves anticorrosion performance. Different inhibitor encapsulation techniques have been studied, including polyelectrolyte and polymer microcapsules, sol−gel nanoparticles, porous silica, nanotubes, and other methods (2, 17−24). In this paper, we describe the use of halloysite clay nanotubes of 50 nm diameter and ca. 1 μm length as containers for the loading, storage, and sustained release of benzotriazole. Extended controlled release was achieved through formation of the stoppers at the tube openings. Benzotriazole release time in water was determined to range from 10 to 100 h depending on the stopper formation at the cylinder ends. These clay nanocontainers containing entrapped benzotriazole were determined to improve the anticorrosion performance of coatings, as demonstrated for both aluminum and copper samples.

MATERIALS AND METHODS

Reagents. Halloysite tube samples were obtained from the Dragon Mine in Eureka, UT (Atlas Mining Co). Benzotriazole was purchased from Sigma-Aldrich. All of the salts, $CuSO_4 \cdot 5H_2O$, $CoCl_2 \cdot 6H_2O$, $FeCl_2 \cdot 4H_2O$, and $FeCl_3 \cdot 6H_2O$, were purchased from Fluka Chemika of Switzerland as dry powders. Industrial oil-based blue paint based on ECS-34 powder was purchased from Tru-Test Co.

Instrumentation. Halloysite samples were characterized by a scanning electron microscope (Hitachi S 4800 FE-SEM) to observe nanotube external surface morphologies. An elemental composition of halloysite samples was determined by using SEM EDX elemental analysis. Electrons were accelerated at 5−15 kV for imaging purposes and at 25 kV for EDX elemental analysis. Halloysite samples were coated with 1.6 nm thick platinum by a Cressington sputter coater (208HR) before each SEM experiment. Samples were coated at 80 mA current for 1 min. The internal hollow lumen of the halloysite was analyzed by using a transmission electron microscope (TEM, Zeiss EM 912) at 120 kV accelerating voltage for electrons. The halloysite surface charge and average effective diameter in colloidal solutions are determined by using microelectrophoresis with a

[†] Louisiana Technical University.

[‡] Glen Muir Technologies Incorporated.

[§] Max Planck Institute for Colloids and Interfaces.

Received for review March 25, 2009 and accepted May 31, 2009

DOI: 10.1021/am9002028

Scheme 1. Loading Procedure of Halloysite Nanotubes with Benzotriazole

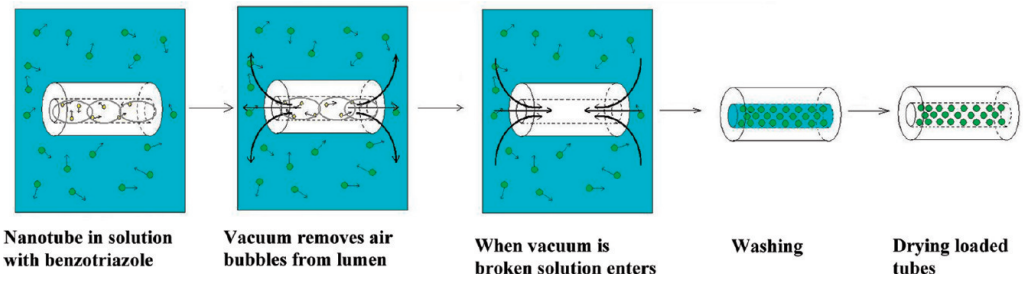

ZetaPlus Potential Analyzer (Brookhaven Instruments). A UV−vis spectrophotometer (Agilent 8453) was used to determine benzotriazole concentration in aqueous media during release experiments. Solutions were calibrated relative to pure DI water before each experiment. Benzotriazole concentration was measured by the intensity of the signal at 265 nm in the UV spectrum. The wettability of the halloysite, as well as its compatibility with paint, was checked with a contact angle measurement system (Future Digital Scientific Co.). For this purpose, a tiny droplet of paint or water (~0.5 μL) was dropped onto a pressed halloysite tablet and the contact angle of the droplet at the liquid−halloysite interface was measured. An Eppendorf 5804R centrifuge was used to separate halloysite nanotubes from colloidal solutions. The solution was centrifuged at 7000 rpm for 2 min for effective separation. A light microscope (Olympus, Japan) with video camera (Sony SSC DC 80) was used to observe corrosion spots on the scratched metal surface. The image was magnified by 10−15 times. A tensile stress instrument (ADMET, EP-0801161-M-48 VAC) was used to determine tensile strengths and the stress−strain relationship of the halloysite−paint composites. Samples were pulled at a speed of 0.3 mm/min for obtaining the stress−strain curve. A scanning vibrating electrode instrument (SVET, Applicable Electronics) was used to detect corrosion current intensity from the corrosion spots of the coated metal samples.

Nanotubule Loading Procedure. To entrap benzotriazole, halloysite was mixed as a dry powder with a saturated solution of benzotriazole in acetone (80 mg/mL). A beaker containing a benzotriazole and halloysite suspension was transferred to a vacuum jar, which was then evacuated using a vacuum pump. The slight fizzing of the suspension indicated that air was being removed from the core of the halloysite tubules and replaced with solution. The suspension was kept under vacuum for 1−5 h and then was cycled back to atmospheric pressure (Scheme 1). This process was repeated three times in order to increase the loading efficiency. Finally, halloysite nanotubes were separated from solution by centrifugation and washed with water. Loading of benzotriazole from its melt and aqueous solutions was also performed but was found to be less efficient (probably because of lower water benzotriazole solubility as compared with acetone).

Benzotriazole Release Kinetics. The release kinetics was investigated in water at pH 6−7 and room temperature. The suspension of halloysite nanotubes was constantly stirred with a magnetic stirrer during the release process in order to establish equilibrium conditions and to increase the release rate. Samples for analysis were separated from the tube suspension by centrifugation. The concentration of benzotriazole was determined by UV spectrophotometry. Complete release (assumed 95%) was checked after 1 h sonication of the halloysite samples at the end of each release study.

Tube Stopper Formation. The formation of stoppers at the tube ends was based on the reaction between loaded benzotriazole and transition-metal ions, which diffused into the tube openings to form insoluble metal−benzotriazole complexes that act as stoppers for the benzotriazole contained in the tubules. For this purpose, benzotriazole-loaded halloysite samples were exposed for 1 min to the bulk aqueous solution containing Cu(II) or other ions. This suspension was constantly stirred with a magnetic stirrer. The processed nanotubes were separated from solution by centrifugation.

Corrosion Resistance Testing. ***Initial Stages of Corrosion Process.*** The initial corrosion on the metal surface was analyzed by the scanning vibrating electrode technique (SVET) (25). Because of electrochemical reactions during corrosion, both anodic and cathodic sites developed on the substrate surface. A PtIr electrode with a Pt-blackened high-capacitance microtip was positioned above the sample. A piezo element generates vibration of the electrode. An alternating current signal is induced because of the electrostatic potential gradient inside the electrolyte solution. The ac voltage was analyzed with a phase-sensitive detector and amplifier (PSDA), and the amplitude was recorded for different horizontal positions of the tip above the sample. The Pt-blackened electrode tip had a diameter of 20 μm and a capacitance of 6.6 nF and was held at 0.3 mm above the sample during scans. The metal plates were fixed on a glass holder and immersed into 0.1 M NaCl aqueous solution. An area of 3 × 3 mm^2 was scanned. Two metal strips made of 2024 aluminum alloy or copper were coated by ZrOx−SiOx sol−gel film or painted with and without benzotriazole-loaded halloysite nanotubes and artificially scratched. The corrosion process was monitored by measuring corrosion current density from the scratched surface over 24 h.

Corrosion Process. The process was also studied by visual microscopy of corrosion development in the scratched area. In this study, 110-Cu alloy strips were coated with ECS-34 True-Test oil-based industrial blue paint. Copper samples were treated with nitric acid solution (20% by weight) to remove impurities from the surface and to polish the metal surface. Then samples were washed with water and dried. After being dried, one of the samples was coated with paint containing benzotriazole-loaded halloysite and another sample was painted without halloysite. The samples were dried in air for 2 days, artificially scratched, and dipped into corrosive solution simulating seawater and containing 24 g/L of NaCl, 3.8 g/L of $CaCl_2$, and 2 g/L of Na_2SO_4 for 10 days as described elsewhere (23, 24). After 10 days, scratched surfaces were analyzed by optical microscopy.

Paint Composite Coating Tensile Stress. Five different paint samples were prepared by the addition of halloysite at different loading ratios in an industrial paint. The paint composite was sonicated for 5 min and thoroughly mixed to homogenize the suspension. Thin aluminum foils were painted with the coatings that contained the different halloysite loadings and dried for 1 week. The dried paint film was released by etching the foil in 0.1 M NaOH solution, dried in air for 3 more days, and tested for tensile stress. The dimensions of the paint film samples were 5.5 ± 0.5 mm width, 13.0 ± 0.5 mm length, and 0.25 ± 0.04 mm thickness.

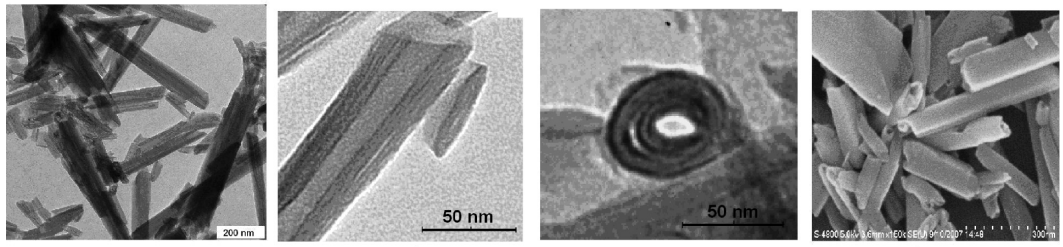

FIGURE 1. (a, b, c) Transmission electron microscopy and (d) scanning electron microscopy images of halloysite nanotubes.

RESULTS AND DISCUSSION

Clay Nanotubes. Halloysite ($Al_2Si_2O_5(OH)_4 \cdot nH_2O$) is a two-layered (1:1) naturally occurring aluminosilicate clay that exhibits a hollow tubular structure in the submicrometer range, and it is chemically similar to kaolin (18−24, 26, 27). When $n = 2$, it is in the form of hydrated halloysite-10 Å with one layer of water molecules between the multilayers. At $n = 0$, the structure is dehydrated halloysite-7 Å, which may be obtained through an irreversible phase transition with loss of adsorbed water as the halloysite is heated to 100−120 °C. Being available in thousands of tons, these nanotubes can be used in a wide area of applications, especially in cases where the geometry of the particles is important. We will discuss further the dehydrated halloysite-7 Å and for simplicity call it halloysite. The size of halloysite tubules varies within 0.5−1.5 μm of length, ca. 15 nm of inner diameter, and ca. 50 nm of external diameter (Figure 1). There are 15−20 aluminosilicate layers rolled in the multilayer tubule walls with a layer spacing of 0.72 nm for the dehydrated halloysite (19, 21). Halloysite forms by kaolinite layer rolling because of the action of hydrothermal processes (19). In halloysite, the SiO_2 layer is relevant to the outer surface of the tube and is negative above pH 4, whereas the Al_2O_3 layer is relevant to the inner lumen surface, which results in a positively charged interior of the tubes at pH less than 8.5 (20, 28).

Sustained Benzotriazole Release from Clay Nanotubes. SEM analysis showed that the halloysite samples contain fine nanotubes with 50 ± 10 nm external diameter and 15 ± 3 nm internal diameter. The length of the tubes is 1000 ± 500 nm. A typical overage halloysite particle size determined from light scattering (based on the tube radius of gyration describing 3D averaging) is 330 ± 10 nm, and the polydispersity is 0.193. Halloysite nanotubes have an electrical ζ potential of −42.6 ± 2 mV in water at pH 6.5, which predominantly corresponds to the silica outermost potential. The chemical composition of a typical halloysite sample is as follows: 17.7% Al, 18.3% Si, 63.7% O, and 0.3% Fe. Loading of the halloysite nanotubes with anticorrosion agents was based on vacuum cycling of a halloysite suspension in a saturated solution containing benzotriazole, as was described earlier (23, 24). The air located in the cores of the tubes was replaced by the anticorrosion solution during this process (Scheme 1). This cycle was repeated three times in order to get the highest loading.

To optimize the benzotriazole solvent for the most efficient loading, we took into account the solubility of benzotriazole and the low viscosity of the solution. In addition, because halloysite nanotubes are hydrophilic (with SiO_2 outermost), the solvent has to be polar for better suspension stability. The loading of benzotriazole into the tubes was possible from its saturated solutions in water and acetone and from melt benzotriazole. We found acetone to be the best solvent for loading in our process, and it allowed more than 4.5% of loading efficiency of halloysite by weight, which is approximately 90% of the theoretical limit (tube lumen volume consists 10% of the total volume, and halloysite density is 2.65 g/cm^3 (18)). Loading benzotriazole from water solution or from its melt resulted in less benzotriazole content, 2.1% and 0.25% by weight, respectively. The higher loading of benzotriazole from acetone as compared to that from water is in contrast to the fact that water wets halloysite better than acetone, which was verified by the higher stability of halloysite colloidal solution in water as compared to that of acetone. The reasons for the higher loading of benzotriazole may be listed as follows: (a) a concentrated solution of benzotriazole in acetone was used (∼10 wt %), whereas benzotriazole is soluble in water only up to ∼0.5 wt %; (b) acetone has a lower viscosity compared to water and benzotriazole melt, and this leads to a higher diffusion rate of benzotriazole into halloysite pores; (c) acetone dries more quickly than water, and under applied vacuum (during the loading procedure) fast evaporation of acetone increases the concentration gradient between internal lumen and external solution, which enhances loading. In the following experiments, we used acetone as a solvent for benzotriazole loading. Loaded halloysite may contain benzotriazole for a long time until it is exposed to water (for example, in the coating defect points). Once the coating integrity has been compromised, the corrosive solution reaches the entrapped inhibitor and active release begins, resulting in the initiation of benzotriazole inhibition.

In Figure 2, extended release profiles of benzotriazole from halloysite nanotubes in water are elucidated. For comparison, benzotriazole dissolution in water is also shown (dissolved by adding it as a powder into water): it is an almost vertical line close to the y axis, indicating very rapid dissolution. The benzotriazole release curves from two typical halloysite samples are close and demonstrate almost complete release of benzotriazole in water within 40 h. The approximately 30% initial bust release of benzotriazole is typical for different molecules loaded into the clay nanotubes

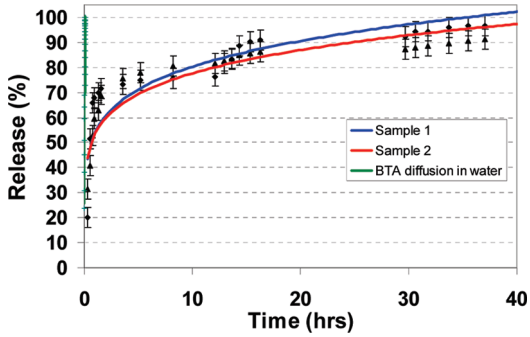

FIGURE 2. Benzotriazole release profiles from two halloysite samples from different batches (water, pH 6.5).

and may be due to the fast dissolution of the material stored in tube fines and in the natural surface pocket and the end of the loosely rolled surface clay sheets (Figure 1).

The benzotriazole release profile from halloysite was fit to the Peppas model (30) $M_t/M_\infty = kt^n$, where M_t is the amount of material released at time t, M_∞ is the amount of material released at infinite time, n is the exponent characteristic of the release mechanism, and k is a constant. The values of k and n are equal to 53.3 ± 0.3 and 0.16 ± 0.01, respectively, for benzotriazole release from halloysite. This is the indication that the diffusion of benzotriazole from both of the halloysite samples takes place according to the same mechanism: i.e., the release of the corrosion inhibitor is determined by the geometry of the tubes rather than the chemistry of the tubule walls. For example, the content of iron oxide in the samples varied from 0.3 to 2.8% (for the first and second samples, respectively), but this did not influence the release profile. Very fast diffusion of benzotriazole from naked crystals fits to the model with k and n equal to 514.4 and 0.64, respectively. These large coefficients k and n may be related to the higher diffusion coefficient of benzotriazole in bulk aqueous solution as compared to that of halloysite tubule lumen. Lower diffusion coefficients in nanotubes may be related to the increased viscosity of water in halloysite nanopores because of its interaction with the tubule inner wall surface. Therefore, sustained benzotriazole release was obtained with approximately 70% of the initial material released within the initial 5 h, and the remaining 25% of the benzotriazole was released in the following 30 h. In the following section, we will describe the use of tube end stoppers to decrease the initial release rates.

Halloysite/Paint Nanocomposite Coating. In Figure 3, SEM micrographs of halloysite nanotubes in a scratched paint layer are shown. Nanotubes are exposed to the external environment at a paint scratch or cracks. Benzotriazole-loaded halloysite will start enhanced release of the inhibitor when a crack occurs, protecting the metal underneath from corrosion process development.

Halloysite is readily mixed with a variety of metal protective coatings, which is an important advantage of this material. Water contact angles for halloysite pressed in the tablet were found to be as low as 10 ± 3°, but the material was still mixing well with paint. Surprisingly, for the paint droplet, the contact angle was even less, ca. 3°. The paint

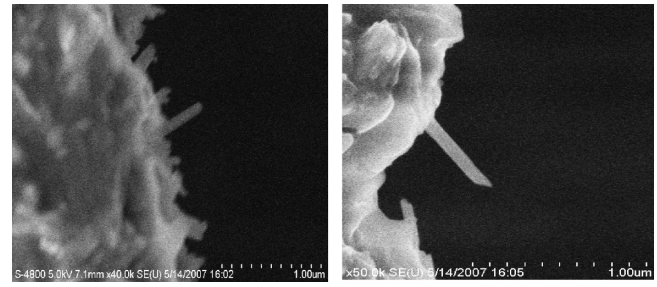

FIGURE 3. SEM micrographs of a paint scratch containing 5 wt % of halloysite nanotubes in it.

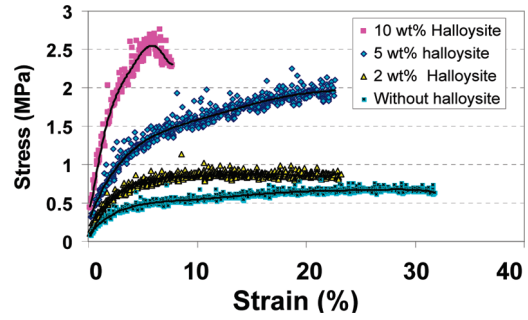

FIGURE 4. Stress–strain relationship of industrial oil-based blue paint.

droplet spontaneously spreads over a halloysite tablet, which is an indication of the good wettability of the halloysite tablet by paint. The presence of undisclosed surfactant additives in the paint may be the reason for this good wettability. Another reason could be due to specific chemical interactions between halloysite surface OH groups and paint hydrocarbon molecules. This interaction could be analogous to the interaction between water molecules and hydrocarbon chains as was described in various publications (31, 32), where polar OH groups interact with the local charges of the CH groups formed because of the electronegativity difference between carbon and hydrogen atoms.

Addition of nanotubes into industrial oil-based paint significantly improved the strain–stress characteristics of the coating, as is demonstrated in Figure 4. A 3-fold increase in paint tensile strength was observed with addition of 5 wt % halloysite (0.7 MPa for pure paint versus 1.9 MPa for 5 wt % halloysite-loaded paint). Halloysite filler also increases the hardness of the paint. Elastic modulus values of the dry paint samples were 16.3 MPa for a layer of pure paint and 23.1, 34.6,and 69.3 MPa for 2, 5, and 10 wt % composites of halloysite with paint, respectively. However, paint films became brittle with more than 10 wt % halloysite loading. These data correspond to results on halloysite clay/polymer bulk composites. For example, incorporation of 5–13 wt % of halloysite in polypropylene resulted in a 30–50% strength increase (26, 27). Therefore, for optimal cover strength halloysite addition into paint should be below 10 wt %. In the Supporting Information, we give an estimate of the minimum halloysite concentration in paint that still provides a sufficient amount of anticorrosion agent for protection, and the sufficient amount is below this value for most of the cases.

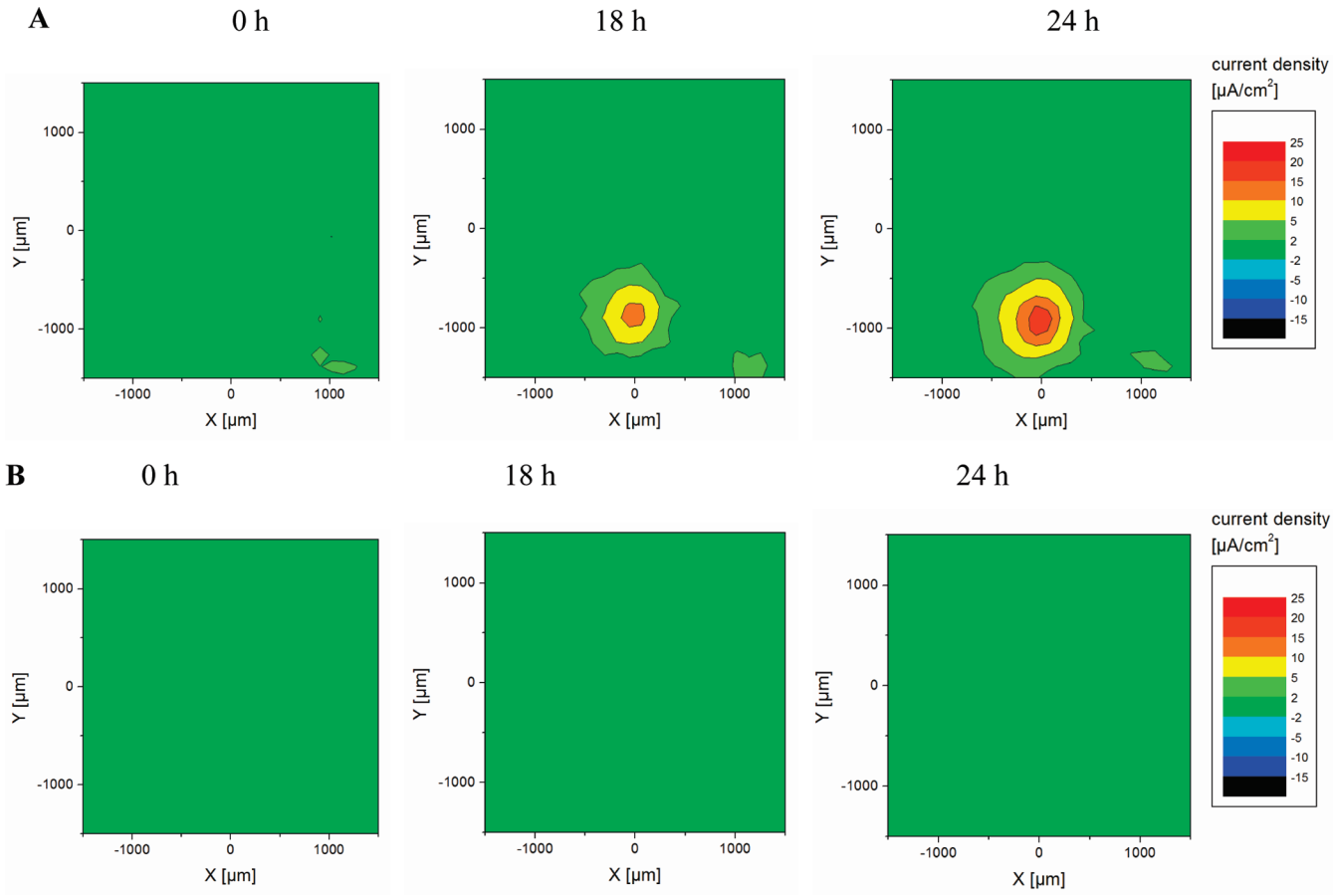

FIGURE 5. Corrosion current densities of 2024-Al alloy coated with (A) pure sol–gel and (B) sol–gel particles containing halloysite loaded with benzotriazole.

Scheme 2. Illustration of Stopper Formation at Halloysite Tube Endings by Interaction of Leaking Benzotriazole with Cu(II) Ions

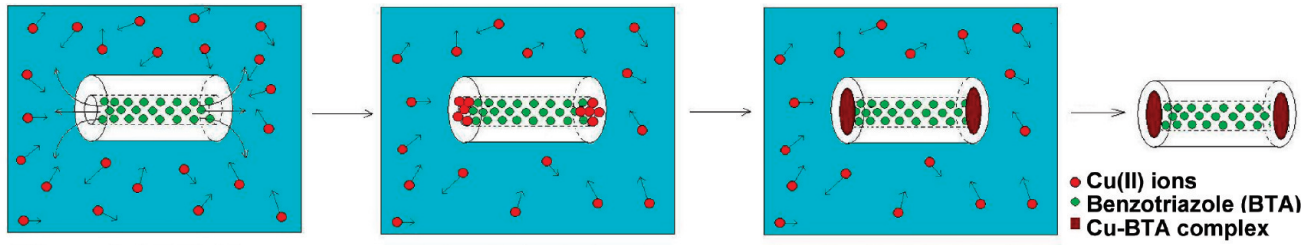

Enhanced Corrosion Protection with Benzotriazole-Loaded Halloysite. The initial stages of corrosion development in metal coatings and the self-healing ability of the halloysite-doped film were analyzed by the scanning vibrating electrode technique on 2024-Al alloy (taken as a substrate), which contains 4 wt % copper. Alloy plates were coated by a dip-coating procedure with a ZrOx–SiOx sol–gel layer and artificially scratched in a similar way. Both samples with and without inhibitor-loaded halloysites were immersed in corrosion solution, and corrosion development was observed over 24 h as maps of the corrosion current.

Anodic corrosion activity on the aluminum alloy coated by a simple sol–gel layer was high and rapidly increased within several hours (Figure 5) in the scratched area. This indicates a fast pitting corrosion process taking place at the artificially introduced defect. In the case of alumina coated with sol–gel-containing halloysite tubes filled with benzotriazole, the rate of corrosion at the defect points is strongly slowed down in the first moment of corrosion and almost no corrosion current (both cathodic and anodic) was developed. In comparison to the pure sol–gel coating, the maximum current density in this case was 6 times smaller (ca. 3 μA/cm^2 for inhibitor-containing sol–gel and 18 μA/cm^2 for pure sol–gel after 24 h of immersion), which indicates a very strong anticorrosion self-healing effect caused by controlled release of the inhibitor from the halloysite nanotubes in the cracked area.

In another experiment, scratched copper strips coated with industrial oil-based paint with or without loaded halloysite were studied. Both of these strips were exposed to a highly corrosive environment simulating seawater for 10 days. Images show that paint containing benzotriazole-

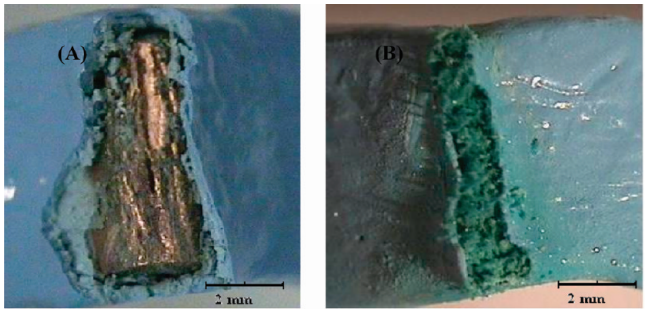

FIGURE 6. Images of scratched copper strips painted with oil-based blue paint (A) containing halloysite nanotubes loaded with benzotriazole and (B) without these tubes, after exposure to a corrosive environment for 10 days.

loaded nanotubes effectively slowed down copper corrosion, because no evidence of rust is visible in the scratched area.

Elemental analysis of the reacted corrosive solution also demonstrated that 128 ± 1 ppm of Cu(II) ions was dissolved for the sample B, whereas no copper was detected for sample A with halloysite-loaded coating. This result is an indication that entrapment of benzotriazole into paint using halloysite nanocontainers is efficient for metal corrosion inhibition, especially when the scratched surface is exposed to a highly corrosive liquid such as seawater. However, a longer release rate for benzotriazole may be needed for applications, and it was reached with tube stopper formation, as is described in the following section.

Tuning of the Benzotriazole Release Rate. Controllable release of benzotriazole from halloysite nanotubes was achieved by the formation of metal−benzotriazole complex caps at halloysite tube endings by the interaction of leaking benzotriazole and metal ions from the bulk solution. The suggested method requires only a short rinsing of benzotriazole-loaded halloysite nanotubes with an aqueous solution containing metal ions.

In Scheme 2, formation of stoppers at halloysite tube openings is demonstrated (using Cu(II) ions). The complex of copper ions and benzotriazole has been well-studied by various authors and described in the review by Cease et al. (3). Benzotriazole forms stable 2D complexes with most of the transition metals, and we tried Cu(II), Fe(II), Fe(III), and Co(II) salts for the stopper formation.

Benzotriazole release characteristics were studied in detail, with formation of stoppers with Cu(II) ions providing the best release control. The decrease in benzotriazole release rate depends on a number of parameters, such as the chemistry and morphology of halloysite samples (we tried halloysite from two different deposits), the concentration and type of metal ion, and the concentration of benzotriazole available at tube openings.

One of the important parameters influencing benzotriazole release rates is the concentrations of metal ions that are used for the formation of metal−benzotriazole stoppers. To determine the influence of metal concentration in the bulk solution on the benzotriazole release rate, we used copper sulfate solutions of six different concentrations to encapsulate benzotriazole inside halloysite tubes (Figure 7a). The benzotriazole release rate constantly decreased by using higher concentrations of copper sulfate solution. This is an indication that the efficiency of the encapsulation strongly depends on the concentration of the metal ions used for formation of the stoppers. This effect may be exploited to develop the desired release rate. For example, the total release time for the sample process with 2 mM of $CuSO_4$ solution reached ca. 100 h. Another important factor that influences benzotriazole release rate is the concentration of benzotriazole at the tube endings available for formation of metal−benzotriazole films. This can be controlled by washing loaded nanotubes with DI water after loading them with benzotriazole and prior to processing them with metal ions. To demonstrate this, we washed nanotubes two times in the first sample and four times in another sample before exposure to 8 mM copper sulfate solution. This allowed less benzotriazole in the reaction zone at the tube ends and "weaker" stopper formation. Evidently, tubes washed two times with water showed slower release as compared to those washed four times before exposure to Cu(II) solution (Figure 7b).

LbL (layer-by-layer) polyelectrolyte encapsulation of halloysite nanotubes was also tried in order to decrease the benzotriazole release rate. An alternate adsorption of cationic poly(ethyleneimine) and sodium poly(styrene sulfonate) was used for this, as described in ref 22. However, a polyelectrolyte multilayer shell did not slow down benzot-

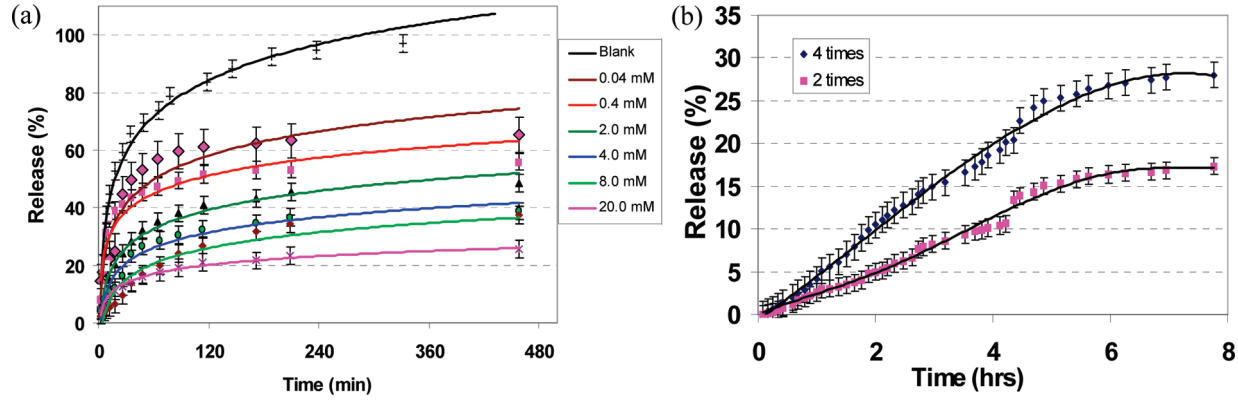

FIGURE 7. (a) Benzotriazole release profiles from halloysite washed with $CuSO_4$ solutions of different concentrations. The release of benzotriazole from untreated halloysite is also shown for comparison. (b) Benzotriazole release profiles from halloysite having Cu−benzotriazole stoppers with 2 and 4 washing stages.

riazole release from the tube. Probably, benzotriazole molecules, which have molecular weights of 119 Da, are too small and the wall of four to five polyelectrolyte layers is too loose to decrease their diffusion essentially. This is in contradiction with our previous results on the entrapping of a higher molecular weight drug, dexamethasone, with LbL-encapsulated halloysite (28, 29).

CONCLUSION

Halloysite nanotubes are promising materials for the entrapment of corrosion inhibitors into paint due to their viability and compatibility with a variety of water- and oil-based coatings. Halloysite is also a "green" material, and because it is a natural product, it will not add risk to the environment. Benzotriazole was loaded in 50 nm diameter halloysite tubes and admixed to paint coatings in the amount of 2−10 wt %. The tensile strengths of such nanocomposite paint coatings increased by approximately 2−4 times. Benzotriazole release from raw halloysite nanotubes extended for ca. 50 h, and its kinetics was fit with a power function model. The corrosion inhibition efficiency of halloysite nanocontainers for aluminum and copper samples was demonstrated by monitoring the localized corrosion current density on scratches; it could also be determined visually by exposure of a scratched metal sample to a highly corrosive environment, which showed significant reduction in the metal corrosion rate. At the second stage of this tube nanocontainer development, the release rate of benzotriazole was controlled by the formation of metal−benzotriazole stoppers at tube endings. This method provides high halloysite loading efficiency and longer release time, which gives additional possibilities for the process optimization. Therefore, one can adjust the benzotriazole release rate from halloysite nanotubes to obtain the best protective properties of metal coating. This is especially important when the flow of the surrounding water takes place, causing premature release of the corrosion inhibitors from the metal surface.

Acknowledgment. We are grateful to Dmitry Fix (Max Planck Institute for Colloids and Interfaces, Golm/Potsdam, Germany) for help with the SVET experiments. This work was partially supported by the Louisiana Board of Regents ITRS and a post-Katrina Nanotechnology research grant.

Supporting Information Available: Text, a figure, and tables describing the estimated amount of halloysite loaded with benzotriazole to be added to the paint for effective corrosion protection. This material is available free of charge via the Internet at http://pubs.acs.org.

REFERENCES AND NOTES

(1) Gichuhi, T.; Novelli, W.; *Waterborne Symposium Proceedings*, New Orleans, Jan 29−Feb 1, 2008; pp 69−78. The School of Polymers and High Performance Materials and Southern Society for Coatings Technology: Hattiesburg, MS, 2008; pp 47−54.
(2) Shchukin, D.; Zheludkevich, M.; Yasakau, K.; Lamaka, S.; Ferreira, M.; Möhwald, H. *Adv. Mater.* **2006**, *18*, 1672–1678.
(3) Sease, C. *Stud. Conserv.* **1978**, *23*, 76–85.
(4) Faltermeier, R. *Stud. Conserv.* **1998**, *44*, 121–128.
(5) Yin, K.; *Proceedings of 208th ECS Meeting*, Los Angeles, Oct 16−21, 2005; The Electrochemical Society: Pennington, NJ; 2005; p 212.
(6) Ravichadran, R.; Nanjundan, S.; Rajendran, N. *J. Appl. Electrochem.* **2004**, *34*, 1171–1176.
(7) Li, J.; Lampner, D. *Colloids Surf., A* **1999**, *154*, 227–237.
(8) Magnussen, O.; Behm, R. *MRS Bull.* **1999**, 15–23.
(9) Abdullah, A.; Al-Kharafi, F.; Ateya, B. *Scr. Mater.* **2006**, *54*, 1673–1677.
(10) Kester, J.; Furtak, T.; Bevolo, A. *J. Electrochem. Soc.* **1982**, *129*, 1716–1719.
(11) Cao, P. G.; Yao, J. L.; Zheng, J. W.; Gu, R. A.; Tian, Z. Q. *Langmuir* **2002**, *18*, 100–104.
(12) Sanad, S. H. *Surf. Technol.* **1984**, *22*, 29–37.
(13) Babic-Samardzija, K.; Hackerman, N. *J. Solid State Electrochem.* **2005**, *9*, 483–497.
(14) Sayed, S.; El-Deab, M.; El-Anadouli, B.; Ateya, G. *J. Phys. Chem. B* **2003**, *107*, 5575–5585.
(15) Bereket, G.; Pinarbasi, A. *Corros. Eng., Sci. Technol.* **2004**, *39*, 308–312.
(16) Casenave, C.; Pebere, N.; Dabosi, F. *Mater. Sci. Forum* **1995**, *192−194*, 599–610.
(17) Li, W.; Calle, L. M.; *Proceedings of 210th ECS Meeting*, Cancun, Mexico, Oct 29−Nov 3, 2006; The Electrochemical Society: Pennington, NJ, 2006; p 143.
(18) Lvov, Y.; Shchukin, D.; Möhwald, H.; Price, R. *ACS Nano* **2008**, *2*, 814–820.
(19) Joussein, E.; Pitit, S.; Churchman, J.; Theng, B.; Righi, D.; Delvaux, B. *Clay Miner.* **2005**, *40*, 383–426.
(20) Tari, G.; Bobos, I.; Gomes, C.; Ferreira, J. *J. Colloids Interface Sci.* **1999**, *210*, 360–369.
(21) Price, R.; Gaber, B.; Lvov, Y. *J. Microencapsulation* **2001**, *18*, 713–723.
(22) Shchukin, D.; Möhwald, H. *Adv. Funct. Mater.* **2007**, *17*, 1451–1458.
(23) Shchukin, D.; Möhwald, H. *Small* **2007**, *3*, 926–943.
(24) Abdullayev, E.; Shchukin, D.; Lvov, Y. *Polym. Mater. Sci. Eng.* **2008**, *99*, 331–332.
(25) Oltra, R.; Maurice, V.; Akid, R.; Marcus, P. *Local Probe Techniques for Corrosion Research Pages*; Woodhead Publishing Ltd: Cambridge, U. , 2006; pp 12−180.
(26) Li, C.; Liu, J.; Qu, X.; Guo, B.; Yang, Z. *J. Appl. Polym. Sci.* **2008**, *110*, 3638.
(27) Liu, M.; Guo, B.; Zou, Q.; Du, M.; Jia, D. *Nanotechnology* **2008**, *19*, 205709.
(28) Veerabadran, N.; Lvov, Y.; Price, R. *Macromol. Rapid Commun.* **2009**, *30*, 94–99.
(29) Lvov, Y.; Price, R.; Gaber, B.; Ichinose, I. *Colloids Surf., A* **2002**, *198*, 375–382.
(30) Peppas, N. *Pharm. Acta Helv.* **1985**, *60*, 110–111.
(31) Shinoda, K.; Kobayashi, M.; Yamaguchi, N. *J. Phys. Chem.* **1987**, *91*, 5292–5294.
(32) Horvath, A. L. *Halogenated Hydrocarbons, Solubility and Miscibility with Water*; CRC Press: Boca Raton, FL, 1982; Chapter 2, pp 23−391.

AM9002028